A journey of materials development illustrated through shape memory alloy and carbon-based materials

Kinshuk Dasgupta, Madangopal Krishnan and Vivekanand Kain*

Materials Group, Bhabha Atomic Research Centre, Mumbai 400 085, India

The history of materials development for the Indian nuclear energy programme is enriched with innovations towards the journey of self-reliance. During this journey, several spin-off technologies evolved which found important applications in the strategic sector. In this article, a brief account of two such technologies, namely, shape memory alloy (SMA) and carbon-based technologies is given. The Ni–Ti-based SMA has been used in the light combat aircraft, Tejas and the carbon nanotube-based composite has been used in the lightweight ballistic resistant jacket, Bhabha Kavach.

Keywords: Ballistic resistant jacket, carbon nanotube, chemical vapour deposition, light combat aircraft, martensitic phase transformation, shape memory alloy.

Introduction

HOMI Jehangir Bhabha's vision of self-reliance of the Indian nuclear energy programme motivated the indigenous development of materials related to nuclear energy. As the primary resources/ores of most of the elements present in India are lean, the challenges to selectively taking out the metal values associated with the unwanted gangue led to the development of unique extraction processes for each metal, involving various steps like innovative physical ore-beneficiation, selective chemical ore-breakdown techniques, ion exchange, solvent extraction, halogenation, metallothermic reduction, hydrogen reduction, reduction–diffusion, molten salt electrolysis, etc. Expertise was developed in related technologies for melting consolidation and vacuum refining using arc and electron beam melting technologies, ultra-purification using thermal decomposition, iodide refining, electron-beam zone refining, etc. Along with these, fabrication technologies, e.g. powder metallurgy, rolling, extrusion, pilgering, welding, coating and ceramic metallurgy were pursued vigorously and strong groups were developed that contributed significantly. The development of a fundamental understanding of materials, microstructural and mechanical properties characterization at different length scales, structure–property correlations, degradation mechanisms, specifically corrosion, have been a strong point of materials activities in the Bhabha Atomic Research Centre (BARC), Mumbai. The fundamental understanding thus developed in the Materials Group of BARC helped address materials-related issues in plants and gave impetus to develop newer applications with a strong basis.

Over the years, a wide range of activities have been taken up to develop a variety of materials starting from metals, alloys and ceramics to other non-metallic materials and composites. The initial efforts were to develop nuclear materials like uranium, plutonium, thorium and its alloys, zirconium, hafnium, titanium and its alloys, zircaloys, boron, beryllium metal and its alloys, specialty steels and stainless steels, etc. Slowly, the expertise was directed towards development of refractory (niobium, tantalum, vanadium, molybdenum and tungsten) metals and alloys, cobalt, superalloys, rare-earth (samarium, cerium, lanthanum, prosedymium and niodynium) metals and alloys, oxide and non-oxide ceramics (boron carbide), alkali (lithium, magnesium and calcium) metals and alloys, ferro-alloys, metallic and non-metallic glasses, and carbon-based materials. Many of the spin-off technologies developed during this journey in the Materials Group, BARC, found large-scale applications. Here, two such representative technologies are illustrated. One is metallic Ni–Ti-based shape memory alloy (SMA) technology, and the other is non-metallic carbon-based technology.

Shape memory alloys

A SMA is an alloy that can be deformed when cold, but returns to its pre-deformed ('remembered') shape when heated. A deformed and distorted article made of SMAs demonstrates the innate ability to regain its original shape and dimensions when heated (Figure 1).

Ordinarily, SMAs can only memorize the shape of the article at a higher temperature (the 'recovered' shape) and, when 'trained', can also be imprinted with the memory of the shape to be assumed at the lower temperature (the 'deformed' shape). This natural tendency of SMAs, for recouping the original high-temperature shape from a distorted low-temperature shape, is a consequence of the reversible

*For correspondence. (e-mail: vivkain@barc.gov.in)

Figure 1. A 'flower' fabricated from thin sheets of equiatomic Ni–Ti alloy is used to demonstrate the shape memory phenomenon. The flower, which is easily deformed into a 'bud' at ambient temperature, rapidly 'blossoms' or recovers its original shape (and dimensions) on raising the temperature by immersing it into a bowl of hot water.

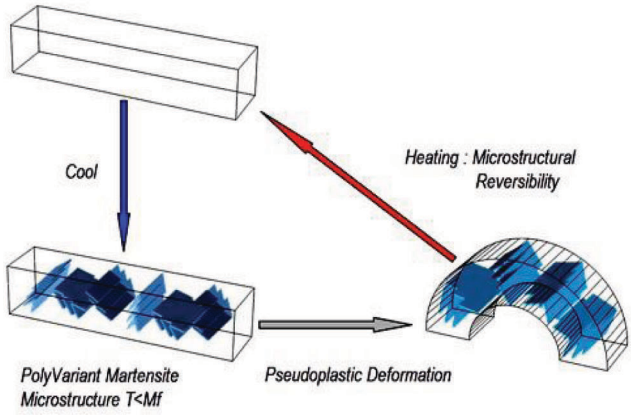

Figure 2. Schematic of the mechanism of the shape memory effect. The phenomenon is the cumulative effect of the ability of the martensitic microstructure of these alloys to provide a 'recoverable' shape change (known as 'pseudoplasticity') and its ability to recover the original parent austenitic crystal orientation (known as 'microstructural reversibility').

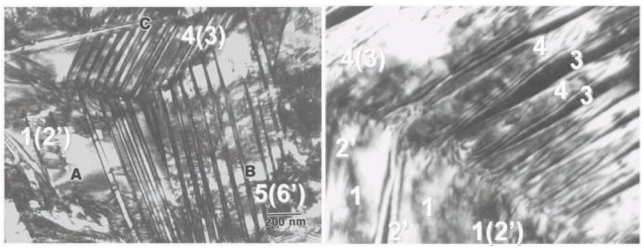

Figure 3. Transmission electron photomicrographs of the microstructure of Ni–Ti alloys. The internally twinned orientation variants of the B19′ martensite are arranged in a self-accommodating architecture with local twinning relationships enforced at the inter-variant interfaces that enable 'pseudoplasticity' and 'microstructural reversibility' necessary to demonstrate the shape memory effect.

nature of the diffusionless martensite phase transformation ('thermoelastic martensite transformation') of the high-temperature austenite phase to the low-temperature martensite phase that occurs during the cooling–heating cycle.

Investigations at BARC on Ni–Ti-based SMAs have shown that the shape memory effect (SME) is the cumulative result of two distinctive properties of thermoelastic martensites, viz. 'pseudoplasticity' and 'microstructural reversibility'[1]. These are the manifestations of the unique crystallographic inter-relationships underlying the martensitic microstructure (Figure 2).

Figure 3 shows the internally twinned orientation variants of the Ni–Ti B19′ martensite that are arranged in a self-accommodating architecture with twinning relationships locally enforced at the inter-variant interfaces. Such a microstructure provides the glissile interfaces necessary for: (1) glide at low applied stress that ensure 'macroscopic' shape change by the rearrangement of orientation variants and without attendant plastic ('unrecoverable') deformation and (2) reversion by coalescence of the polyvariant microstructure into the single crystal orientation of the parent high-temperature phase[2].

Of a reasonably large number of alloys that show SME, Ni–Ti-based alloys are the best in terms of shape memory properties and their viable engineering applications. At this point in time, a fairly wide gamut of medical, engineering, nuclear and space applications of Ni–Ti-based SMAs have been developed that successfully exploit the excellent biocompatibility, superelasticity, shape recovery, damping characteristics and high magnitude of shape recovery stress.

There are a few ways in which shape memory properties could be utilized in practical applications. In 'free' recovery applications, the shape memory phenomenon is utilized merely to recover the original shape, as in the case of the 'flower' in Figure 1. On the other hand, if a deformed SMA object is constrained in a manner as to prevent free recovery, an increase in temperature that instigates recovery of shape will result in the generation of a large 'reversion' stress, in proportion to the extent to which the deformed object strains to regain its original shape. This behaviour of 'constrained recovery' is widely employed in static applications of SMAs such as fasteners, ferrules, couplings and reinforcements, and in dynamic applications such as heat engines and actuators[3].

Research on SMAs has been going on in the Materials Group of BARC for over three decades, which has resulted in several important scientific contributions on material characterization and phase transformation in these materials. Alongside basic research, the development of the preparation and fabrication of SMAs was also pursued, which has led to the successful development of several

Figure 4. Ni–Ti–Fe shape memory alloy (SMA) heat-shrinkable ferrules developed by BARC, Mumbai, have been deployed for application in the Tejas light combat aircraft (LCA).

Figure 5. Superelastic Ni–Ti SMA three-wave springs and Ni–Ti–Fe heat-shrinkable couplings developed for aerospace applications.

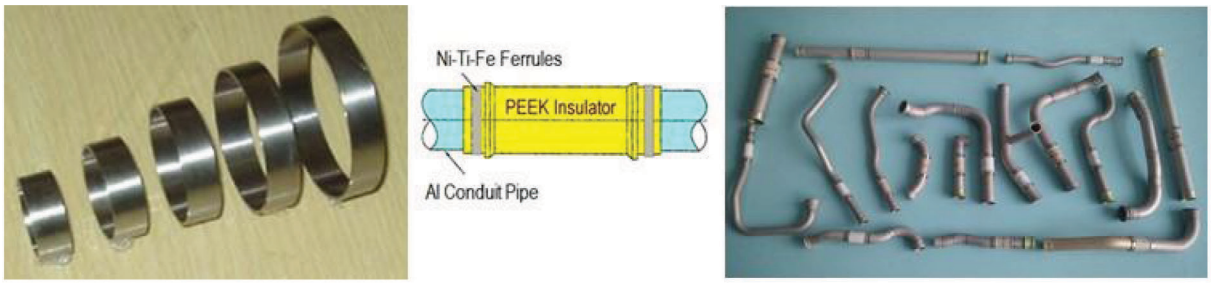

Figure 6. Five sizes of Ni–Ti–Fe heat-shrinkable ferrules developed by BARC for fastening PEEK polymer insulators onto aluminium conduit pipes in Tejas LCA.

Ni–Ti, Cu–Zn–Al, Ni–Mn–Ga, and Fe-based SMAs. However, the outstanding achievement of this endeavour has been the development of Ni–Ti SMAs and Ni–Ti–Fe heat-shrinkable ferrules for the light combat aircraft (LCA), Tejas, designed and manufactured by Aeronautical Development Authority (ADA), and Hindustan Aeronautics Limited (HAL), Bengaluru (Figure 4). The importance of this achievement is highlighted by the fact that, due to the ongoing import restrictions, both alloy and ferrule were not available for the Indian defence and nuclear industries from any foreign manufacturer. Apart from heat-shrinkable ferrules that have been deployed, BARC has also developed Ni–Ti–Fe couplings for joining titanium half-alloy hydraulic tubings and Ni–Ti 'superelastic' three-wave springs for aerospace applications[4] (Figure 5).

SMA fasteners, in particular the heat-shrinkable ferrules developed for Tejas, have several advantages over conventional heat shrink and mechanical interference fasteners, such as a high interference strain arising from the large shape recovery (5–6%), constant recovery stress or 'coupling' stress (300–500 MPa) over the extent of elastic interference strain, a self-adjusting uniform radial pressure, the scope of the application over a wide temperature range (liquid nitrogen to about 300°C) and a relatively low installation temperature (liquid nitrogen to 100°C). These exceptional qualities are crucial to joining or fastening components that are problematic, such as heat-sensitive materials (e.g. electronic circuitry), pyrotechnic materials, low melting materials (e.g. plastics) and also where other conventional joining processes such as welding or brazing are not feasible (i.e. proximity to heat sensitive components or joining of dissimilar alloys).

The Ni–Ti–Fe heat-shrinkable ferrules are designed to clasp PEEK polymer insulators onto aluminium conduit pipes (Figure 6) that are primarily used to convey fuel within the wings, fuselage and drop tanks (Figure 7) of Tejas. The PEEK insulators, which interrupt the continuity of the conduit pipes, are required to ensure safety from static and lightning discharge. Interestingly, the Ni–Ti–Fe SMA ferrule is possibly the only dependable solution

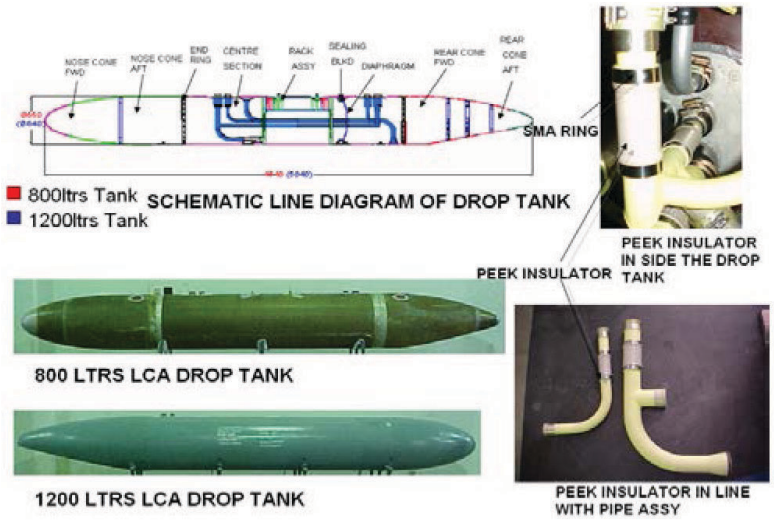

Figure 7. Ni–Ti–Fe heat-shrinkable ferrules used in the drop tanks of Tejas LCA.

Figure 8. The ferrules are expanded under LN2 using a special radial expansion tool and stored in cryogenic flasks until deployment. They are checked with a go-gauge and installed on the joint using a tong. With rise in temperature to ambient, shape recovery ensues and generates a reversion stress that firmly squeezes the PEEK insulator onto the aluminium conduit pipe.

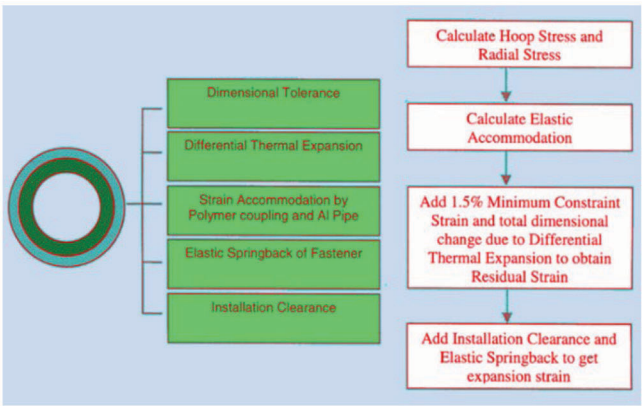

Figure 9. Schematic illustration of the essential components involved in the design of a shape memory ferrule. The dimensions of the unexpanded ferrules ensure that a minimum constraint strain of 1.5% remains after allocations to the elastic yielding of PEEK, differential thermal expansion, dimensional tolerance, etc.

available for joining a polymeric material to a metallic material (dissimilar materials that have vastly different elastic moduli and thermal expansion coefficients), that which provides a large recovery strain, constant interference stress and uniform radial pressure, and also meets the requirement of low installation temperature (within a congested aircraft structure composed of heat sensitive materials).

The Ni–Ti–Fe ferrules are expanded under LN2 to more than 5% residual strain using a special segmented radial expansion tool developed for the purpose, stored until deployment in cryogenic flasks, and installed on the insulator–conduit pipe joint after verification with go gauges (Figure 8). The dimensions of the ferrules, in proportion to those of the PEEK insulator and the aluminium conduit pipes, are such that the complete recovery of its original shape does take place and at least 1.5% pre-strain remains

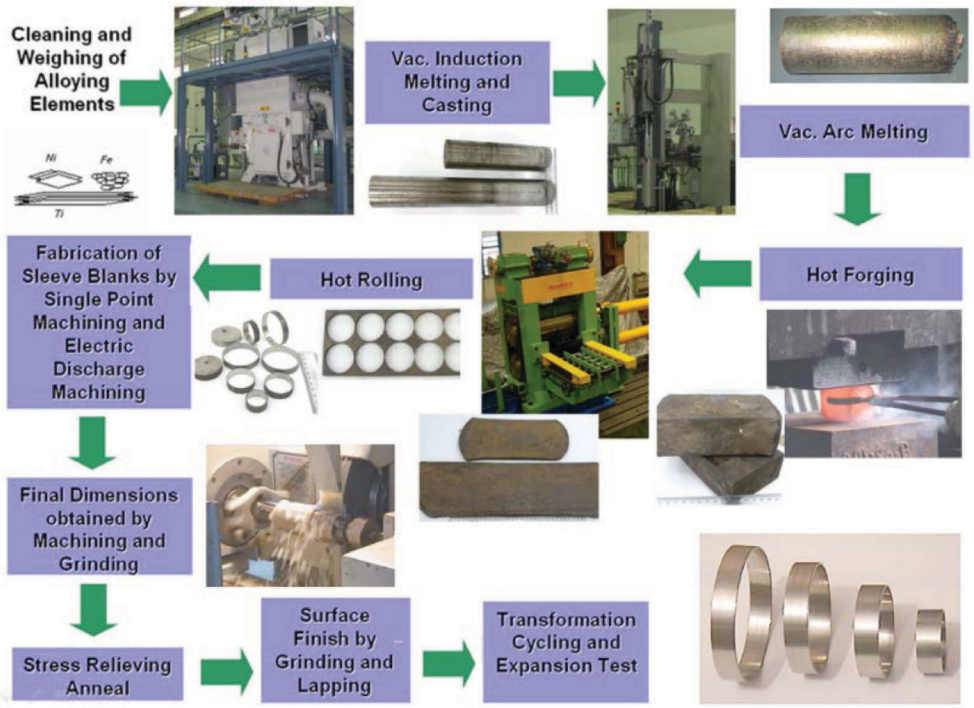

Figure 10. The processing flow sheet developed under the BARC–ADA collaborative project for the production of Ni–Ti SMAs and Ni–Ti–Fe heat-shrinkable ferrules.

unrecovered. In such constrained conditions of shape recovery, a large 'reversion' or interference stress is generated at the joint, which squeezes and tightly fastens the PEEK insulators onto the aluminium conduit pipes.

The dimensions of the recovered or 'unexpanded' ferrules take into account (Figure 9): (1) the 6% 'recoverable' deformation under LN2 and the elastic spring back, (2) the allowable installation clearance, (3) the loss in interference strain on account of dimensional tolerances, differential thermal expansion and elastic accommodation (in PEEK insulator and aluminium conduit pipes), (4) the requirement of 1.5% residual strain, and (5) the design specification of the pull-out load. On the whole, a combination of alloy selection and mechanical design of the ferrules together ensures that nearly constant reversion stress of about 500 MPa is delivered within the service temperature window of –55°C to +150°C.

Based on several trails at BARC, the following flow sheet for the preparation of Ni–Ti SMA preforms, and the fabrication and machining of heat-shrinkable Ni–Ti–Fe ferrules was developed and scaled up to viable production levels (Figure 10): preparation of ingots of Ni–Ti alloy by vacuum induction melting of pure raw materials, consumable vacuum arc remelting of billets, hot hammer forging of blocks, hot rolling of slabs, electric discharge machining (EDM) of blanks, single-point machining and grinding of ferrules, and thermomechanical treatment.

The production activities were spread over different work centres: the induction melting and hot rolling were carried out at the Atomic Fuels Division, BARC; the consumable vacuum arc melting was carried out at the Nuclear Fuel Complex, Hyderabad; the hot forging was done at the Foundry & Forge Division (F&F Div.), HAL, Bengaluru; the machining of the ferrules was carried out at a private workshop in Mumbai, while the thermomechanical treatment and detailed characterization and testing were carried out at Materials Group, BARC. The major innovations in the processing methodologies that established the successful preparation of alloy and ferrule are: (1) design of alloy chemistry with an internal getter for control of composition to within 0.1 at% (or 10°C variation of transformation temperature) and development of suitable crucible coating, raw material charging pattern and melting schedule; (2) optimization of consumable vacuum arc remelting for obtaining fine-grained billets with minimum centre shrinkage and uniform distribution of a specific second phase for obviating hot shortness; (3) optimization of six-side hot hammer forging and hot rolling processes (Figure 11) for completely breaking down the cast structure and to produce slabs with equiaxed grains and pure <111>//ND gamma fibre texture to achieve a uniform and large recoverable strain in ferrules machined through the slab face (Figure 12); (4) thermo-mechanical processing for enhancing shape recovery, recovery stress and fatigue life (Figure 13).

Each Tejas aircraft (including drop tanks) requires about 200–250 ferrules of various sizes. Under three projects received during 1998–2012, over 3000 ferrules of

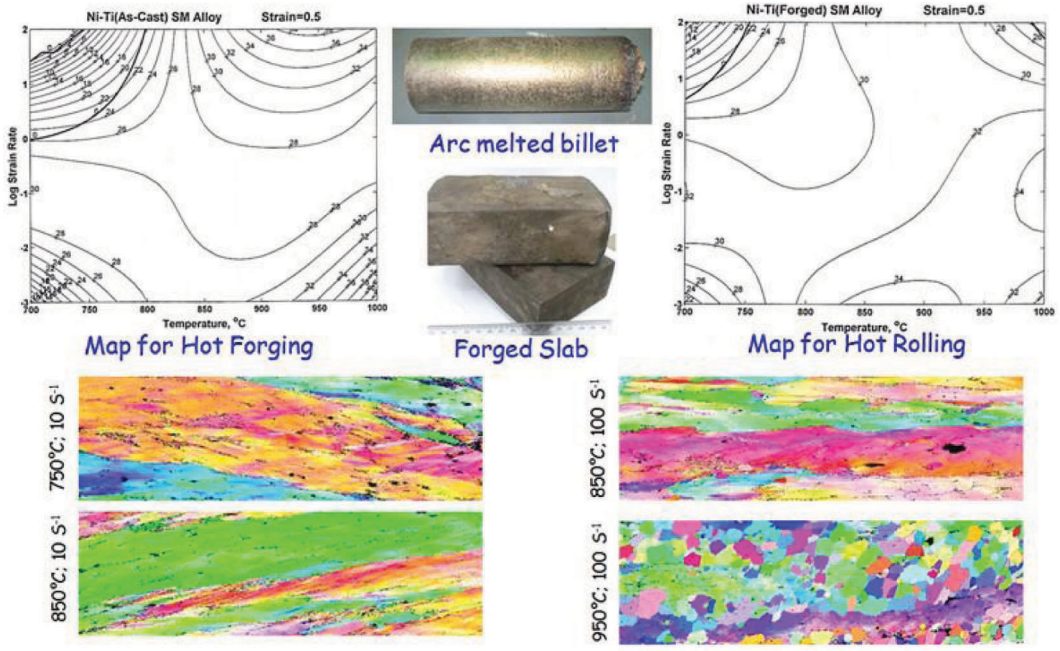

Figure 11. Deformation processing maps and microscopic characterization have been used to identify the strain rate–temperature regimes of dynamic recrystallization (DRX) for breaking the as-cast structure of arc-melted Ni–Ti–Fe SMA by hot forging and rolling to produce slabs of equiaxed microstructure with <111>//ND gamma fibre texture. This has been incorporated into the processing route of Ni–Ti–Fe SMA.

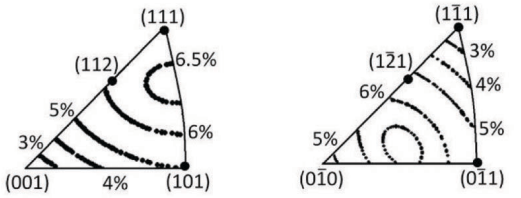

Tensile strain (%)				Compressive strain (%)			
<111>	<110>	<100>	<112>	<111>	<110>	<100>	<112>
5.81	5.08	2.15	6.13	1.97	5.19	4.47	5.28

Figure 12. Equistrain contours of the shape strain reveal that in Ni–Ti alloys, the <111>//ND gamma fibre texture provides a uniform and large recoverable strain in ferrules machined through the slab face. This key understanding forms the basis of selecting the parameters of hot forging and hot rolling route for administering 800–1000% reduction required for breaking and eliminating cast structure.

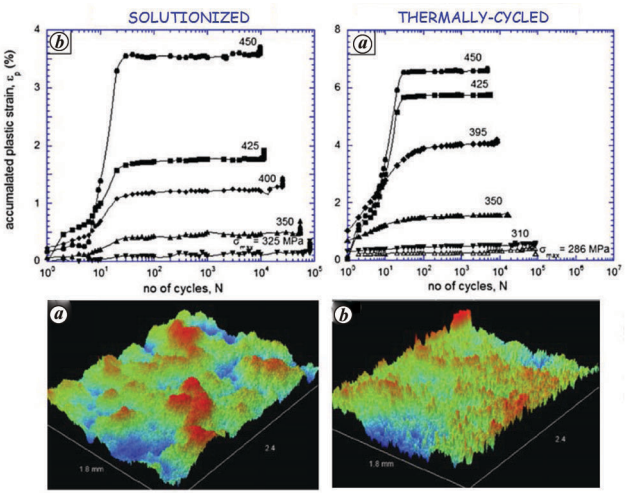

Figure 13. Enhancement in the stress-controlled fatigue life of Ni–Ti–Fe SMAs by nearly 300% is achieved with the aid of transformation cycling. This is attributed to the reduction in the intensity of localized strain due to build-up of dislocation debris through the provisioning of multiple sites for the nucleation of Lüder bands. This thermomechanical treatment has been incorporated into the production route of heat-shrinkable ferrules.

five sizes (20, 25, 32, 40, and 50 mm nominal ID) were designed, manufactured at BARC and supplied to ADA, Bengaluru. These ferrules have been used in equipping at least 15 aircraft of the initial four development versions of Tejas (Technology Demonstrator (TD), Prototype Vehicle (PV), Limited Series Production (LSP), and Naval Prototype (NP), in qualification testing, simulation rigs and in the development of drop tanks.

The required certification for use of SMA ferrules in combat aircraft was received from the Centre for Military Airworthiness and Certification (CEMILAC) after clearing a battery of rigorous tests for airworthiness of the ferrule–insulator–conduit assemblies, such as proof test, burst pressure test, gaseous leak test, impulse test, thermal shock test, vibration test, axial pull-out test, misalignment test, structural relaxation test, tube restraint test, spark/lightning strike test and long-term endurance test involving 140,000 cycles of pressurization under the combined

action of tensile, shear and bending forces. The performance of the component in these tests has given the assurance of its integrity in providing sufficient sealing grip under conditions of stress, temperature and hydraulic pressure, more severe than what is expected to be encountered in service. The fact that there has not been, to date, a single failure or malfunction of these components during testing or during flight, bears testimony to the robust design, processing technology and production procedures.

With a long-term vision of translating the technology of manufacture of Ni–Ti–Fe ferrules to an industry level, a tripartite MoU was signed between ADA, BARC and F&F Div., HAL, in January 2007 for technology transfer and the setting up of a dedicated SMA manufacturing facility. Under the MoU, BARC had undertaken to provide the technology for preparation of (1) Ni–Ti SMA, its preforms and fabrication of ferrules, (2) assist in the purchase and installation of processing equipment such as vacuum arc melting furnace, vacuum induction melting furnace, hot rolling mill, etc., (3) assisting in obtaining certification of Type Approval of the process, and (4) collaborating in new projects. By 2011, a new plant had been set up by HAL at its F&F Div. in Bengaluru (Figure 14), all process equipment were successfully installed and Type Approval certification was awarded by CEMILAC for the production of Ni–Ti–Fe ferrules. As of 2019, HAL had produced about 42 aircraft sets of ferrules for Tejas at this plant.

The most remarkable part of the BARC–ADA collaborative project was that the initial development of Ni–Ti–Fe SMA heat-shrinkable ferrules was achieved in just nine months, which enabled the first flight of Tejas on 4 January 2001. The Ni–Ti–Fe heat-shrinkable SMA ferrule remains the most significant application of smart materials in the domestic Indian scenario. For this achievement, the BARC–ADA team was awarded the prestigious 'Path Breaking Research/Outstanding Technology Development Award' (2011) by DRDO.

Figure 14. SMA manufacturing facility set up at F&F, HAL, Bengaluru, under a tripartite MoU between BARC, ADA and HAL for the transfer of technology of Ni–Ti SMAs and Ni–Ti–Fe heat-shrinkable ferrules.

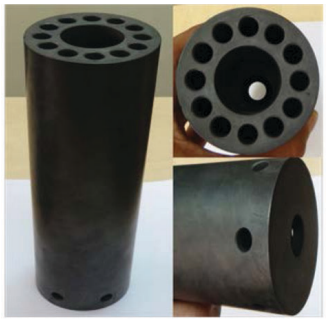

Figure 15. Prototype graphite components.

Carbon-based materials

Carbon is an exotic material with a wide range of structures and properties. It can have crystalline (such as graphite, diamond, carbon nanotube (CNTs)) as well as disordered (such as carbon black, glassy carbon) structures. The bonding in carbon materials may vary from sp^2 to sp^3 hybridization. Carbon materials possess the capability to withstand high temperature (in a protective environment), increased strength up to 2500°C, chemical inertness, low coefficient of thermal expansion, good thermal conductivity, low density and good thermal shock resistance. Carbon nanomaterials have a very high specific surface area, useful for adsorptive separation. The versatility of carbon materials has made them useful for various structural and functional applications in the Department of Atomic Energy (DAE).

Graphite

This is widely used in nuclear as well as non-nuclear applications. Graphite has very high thermal shock resistance and its creep rate is very small below 1500°C. The tensile strength of graphite increases with temperature and is about twice at 2500°C as against room temperature. Graphite does not melt, but sublimes at 3650°C. The low atomic weight with high neutron scattering probability and stability under irradiation has made graphite the right choice as the moderator in high-temperature reactors. The first nuclear reactor CP-1, constructed in 1942 at Stagg Field University of Chicago, USA, used graphite as the moderator. Advanced gas cooled reactors (AGRs), high-temperature gas-cooled reactors (HTGRs), molten salt breeder reactors (MSBRs), and the liquid metal-fuelled reactors (LMFRs) all use graphite moderators[5]. The Indian High Temperature Reactor (IHTR) design uses graphite as reflector[6]. The Indian research reactor CIRUS also used graphite as reflector. Apart from the nuclear field, graphite finds applications as electrodes, dyes and crucibles. Figure 15 shows some prototype graphite components developed at BARC.

Carbon–carbon composite

Carbon–carbon (C–C) composites present a family of materials composed of carbon fibre reinforced with carbon

matrix. The carbon fibre can be reinforced unidirectionally or multidirectionally. Fibre type, lay-up pattern and heat treatment procedures play a predominant role in their properties and subsequent applications. The advantage of C–C composites over graphite is that the properties can be tailored by controlling the fibre architecture and microstructure of the matrix. The main application areas of C–C composites are those which require high strength and light weight and they are mostly used in aerospace, nuclear and defence applications. As C–C composites are an infinitely variable family of materials, the processing and design variables such as (1) architecture, i.e. 1D, 2D, 3D or random fibre distribution; (2) fibre precursor, i.e. pitch, polyacrylonitrile (PAN) or vapour grown; (3) matrix, i.e. liquid impregnation (pitch or resin) or chemical vapour infiltration (CVI) and (4) final graphitization temperature influence the properties and behaviour of C–C composites. Figure 16 shows a general flow sheet adopted at BARC for making C–C composite. Figure 17 *a* and *b* shows the microstructures of PAN-fibre reinforced and carbon black-reinforced C–C composites respectively.

Carbon nanotubes

In recent times CNTs have found many applications due to their exotic properties. BARC has developed two unique facilities for the large-scale production of CNTs. Figure 18 *a* shows a fluidized bed chemical vapour deposition (FB-CVD) reactor that can produce CNTs in powder form at the rate of 1 kg/day. Figure 18 *b* shows another reactor that employs floating catalyst chemical vapour deposition (FC-CVD) technique in order to get CNTs in the aerogel form, wherefrom CNT sheet and CNT fibre can be prepared.

Fluidized bed synthesis of carbon nanotubes: In this method, one needs to fluidize nano-agglomerate particles containing catalysts (generally transition metals or their compounds), using a carrier gas like nitrogen or argon along with a hydrocarbon gas like methane or acetylene.

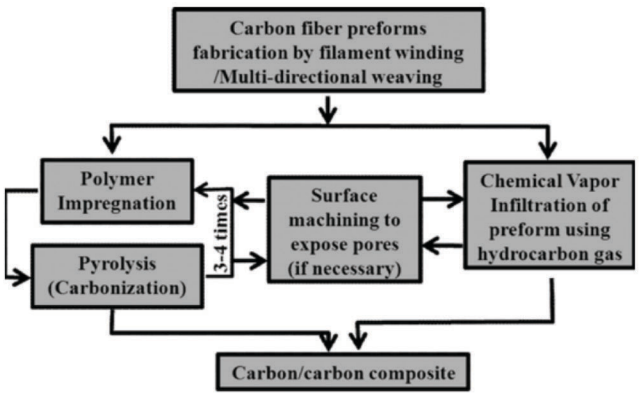

Figure 16. Flow sheet for making C–C composites.

CNTs grow on a catalyst containing nano-agglomerate particles by the decomposition of hydrocarbon. The use of cheap precursors and reduction in the processing steps are the key factors in producing CNTs economically. In order to meet these requirements, carbon black (N 330-grade, furnace black) as the nano-agglomerate particle, ferrocene as the catalyst and acetylene/methane as the precursor hydrocarbon were chosen. The unique feature of carbon black is that it has primary particles of size ~35 nm, which form agglomerates in the size range 80–120 μm and can be easily fluidized. It does not require any processing prior to fluidization. Similarly, ferrocene on cracking in an inert atmosphere deposits nascent iron (Fe) nanoparticles on the carbon black surface and it acts as the catalyst for CNT growth. CNT was grown by catalytic cracking of hydrocarbons (CH_4 or C_2H_2) in the temperature range 700°–900°C. By properly controlling the process parameters, good quality CNTs (>98.5% pure) with a high yield (>92%) could be obtained[7].

Further, these CNTs have been utilized for various applications. A few of them are mentioned below.

Carbon nanotube-reinforced composite for ballistic application: BARC has developed a light-weight ballistic resistant jacket (BRJ), named Bhabha Kavach, where CNTs have been used as reinforcement both in a ceramic matrix and a polymer matrix to enhance their properties. The addition of CNTs in boron carbide (B_4C) tiles that are used as the strike face in the BRJ, could increase their fracture toughness by more than double[8].

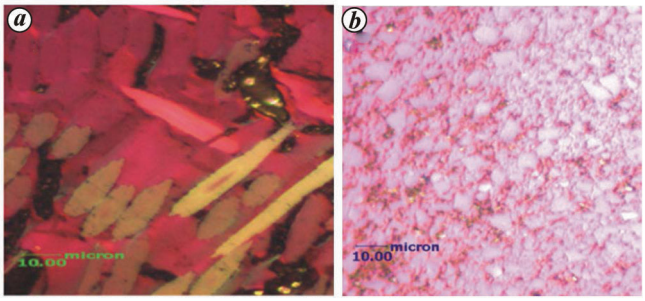

Figure 17. Polarized light photomicrographs of (***a***) PAN fibre-reinforced and (***b***) carbon black-reinforced C–C composite.

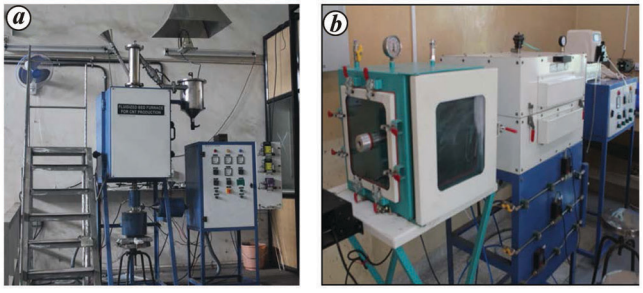

Figure 18. ***a***, Fluidized bed CVD reactor for CNT powder generation. ***b***, Floating catalyst CVD reactor for CNT aerogel production.

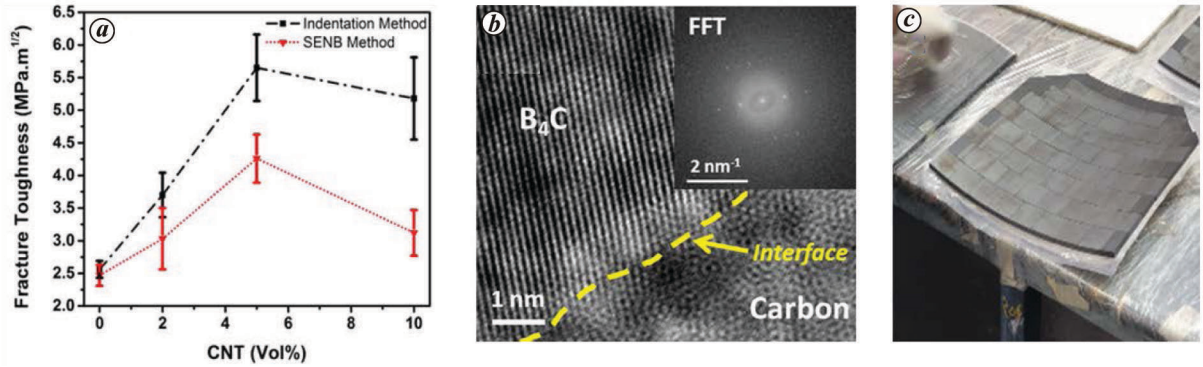

Figure 19. ***a***, Effect of CNT addition on the fracture toughness of B_4C. ***b***, High-resolution TEM image showing the interface of B_4C and CNT. ***c***, B_4C–CNT tiles arranged in a particular fashion (reproduced as a part from ref. 8).

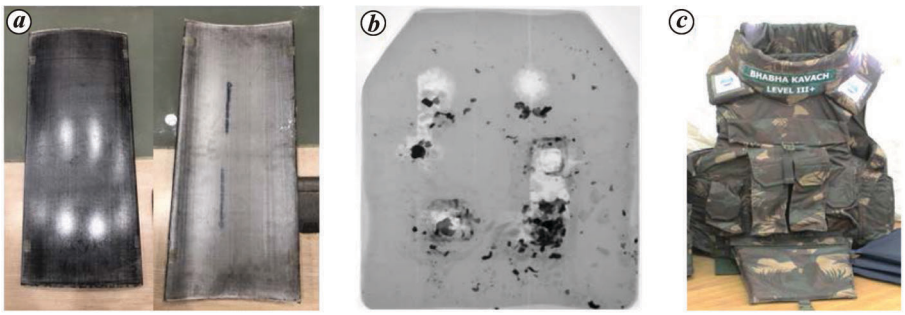

Figure 20. ***a***, CNT–polymer composite used in Bhabha Kavach. ***b***, X-ray radiographic image of a bullet-struck armour panel. ***c***, Photograph of a Bhabha Kavach.

Figure 19 *a* shows the effect of CNT addition on the fracture toughness of B_4C. The optimum amount was found to be 5 vol%. This addition not only improves fracture toughness, but also increases the flexural strength of B_4C and retains its hardness, which in turn provide better ballistic performance. Figure 19 *b* depicts the interface of CNT and B_4C that plays a vital role in the enhancement of properties. Technology has been developed for the production of B_4C–CNT tiles in large quantities by hot-pressing (Figure 19 *c*).

The Bhabha Kavach also utilizes CNT–polymer composites as a backing for the ceramic tiles[9] (Figure 20 *a*). The addition of CNT improves the stiffness and heat transfer properties of the polymer and thus reduces the back-face signature during a ballistic test[10]. An X-ray radiographic image of a bullet-struck Bhabha Kavach armour panel consisting of B_4C, CNT, and polymer is shown in Figure 20 *b* to reveal how the bullets get fractured and trapped into the armour panels. Figure 20 *c* shows a representative image of the Bhabha Kavach.

Carbon nanotube-based composite for metal ion extraction: Extractant encapsulated composite beads made up of CNT, polyvinyl alcohol (PVA) and polyether sulphone (PES) have been utilized for rare-earth extraction (Figure 21 *a*–*c*)[11,12]. CNT addition improves the extraction capacity and rate of extraction several times.

Functionalized CNTs have been extensively used for the separation of lanthanides and actinides[13–15]. Both theoretical studies and practical experiments suggest that task-specific functionalization of carbon nanomaterials is helpful for selective adsorption of lanthanides and actinides onto the surface of the nanomaterials. Water purification also employs CNTs for effective removal of heavy metal ions and other pollutants[16–18].

Carbon nanotube aerogel by floating catalyst chemical vapour deposition: Carbon nanotube aerogel (CNT aerogel) is a self-assembled 3D structure of long CNTs that can be synthesized by FC-CVD. This method is able to retain some of the significant properties of CNTs at macroscale. Generally, a higher temperature (>1200°C) is employed in this process compared to the FB-CVD process. Use of sulphur as the growth promoter is another feature of FC-CVD to produce CNT aerogel[19]. At BARC, CNT aerogel was produced by catalytic cracking of ethanol using Fe as the catalyst and S as the promoter. Figure 22 *a* shows a snapshot during CNT aerogel formation inside the furnace. Depending on requirement, the product can be further collected in the form of wool (Figure 22 *b*), sheet (Figure 22 *c*) or fibre (Figure 22 *d*) by varying the process parameters.

It is possible to control the alignment of CNTs in these macrostructures. Figure 23 *a* shows scanning electron

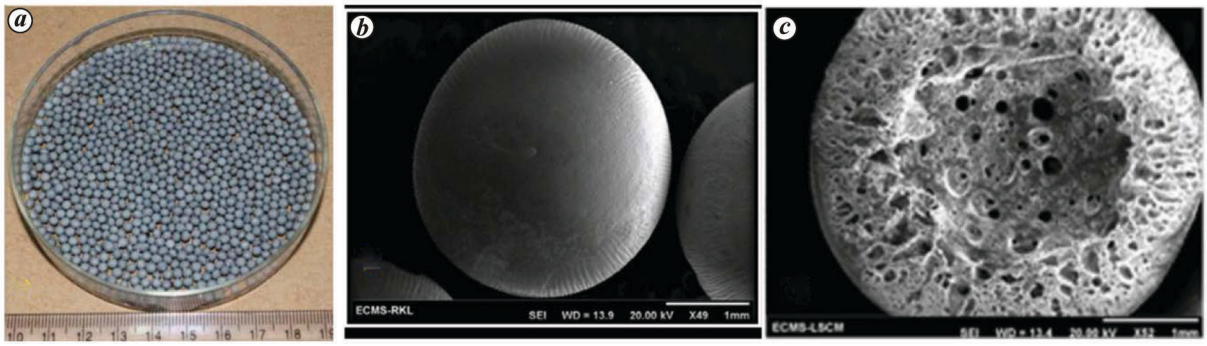

Figure 21. CNT–PVA–PES composite bead showing (***a***) narrow size distribution, (***b***) sphericity and (***c***) cross-section with porous internal structure (reproduced from refs 11, 12).

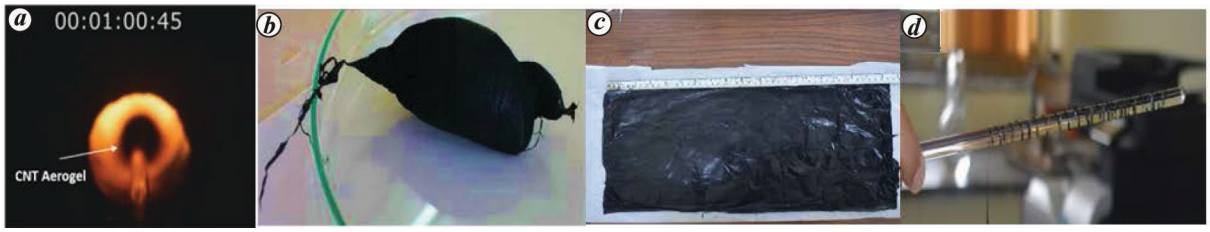

Figure 22. ***a***, Snapshot of CNT aerogel formation. ***b***, CNT wool. ***c***, CNT sheet. ***d***, CNT fibre.

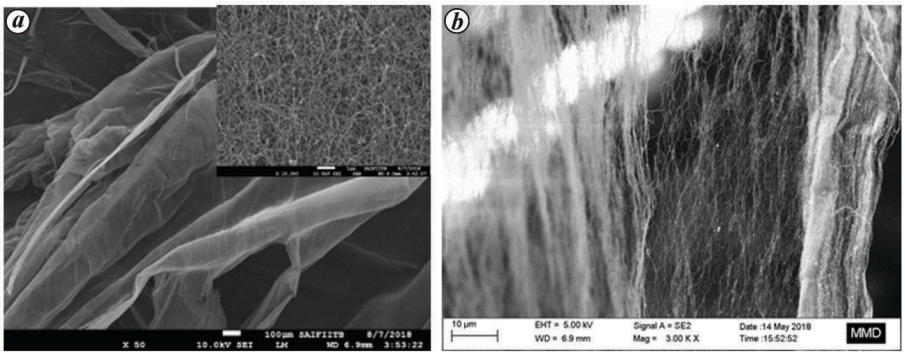

Figure 23. SEM images of (***a***) CNT wool and (***b***) CNT sheet.

photomicrographs of CNT wool, where the CNTs are isotropically oriented (inset). However, in the CNT sheet they are relatively aligned (Figure 23 *b*).

It is also possible to control the type of CNTs in these structures. Depending on the processing conditions, CNTs may be either single-walled (Figure 24 *a*) or multi-walled (Figure 24 *b*), which can be observed from the transmission electron photomicrographs. It can also be observed from the Raman spectra[20]. Single-walled CNTs produce an RBM peak along with a sharp G peak, prominent 2D peak and negligible D peak (Figure 24 *c*). The RBM peak is missing and the D peak is prominent in the case of multi-walled CNTs (Figure 24 *d*).

Few applications of CNT aerogel is described below.

CNT aerogel filter for viruses: Filters have been prepared from the CNT aerogel for trapping nanoparticles, viruses and bacteria (Figure 25 *a*). The average pore size of the CNT aerogel filter is below 100 nm. The efficacy of CNT aerogel-based filter was tested against bacterophage P1, which is a virus that infects bacteria. The phage P1 has a large icosahedral head of approximately 55–85 nm diameter attached to a characteristic long tail of 200–300 nm. CNT aerogel filters were autoclaved (121°C and 15 Psi, 15 min) for sterilization and then used for checking filtration efficiency for P1 phage using the millipore filter assembly and standard procedure. The CNT aerogel filter could trap the bacteriophage with an efficiency comparable to a commercial N95 mask. Figure 25 *b* shows the image of the trapped virus.

Biosensor-based on CNT aerogel: An ultrasensitive label-free biosensor has been prepared from CNT aerogel, which is capable of detecting DNA hybridization rapidly[21]. The multi-directional CNT embedding into the CNT aerogel electrode demonstrated linear ohmic and near isotropic

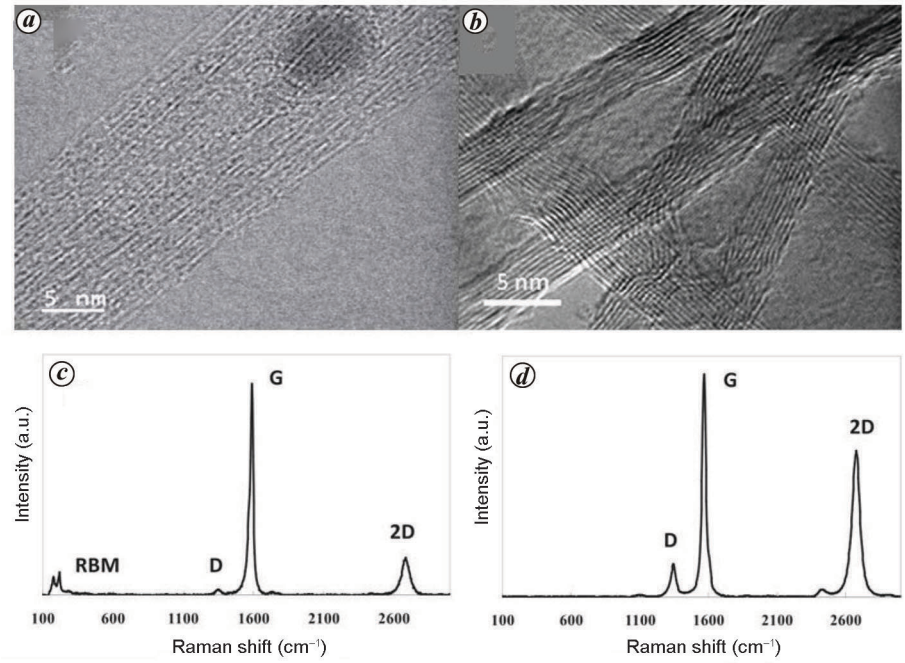

Figure 24. TEM images of (***a***) SWCNT bundles and (***b***) MWCNT. Raman spectra of (***c***) SWCNT and (***d***) MWCNT.

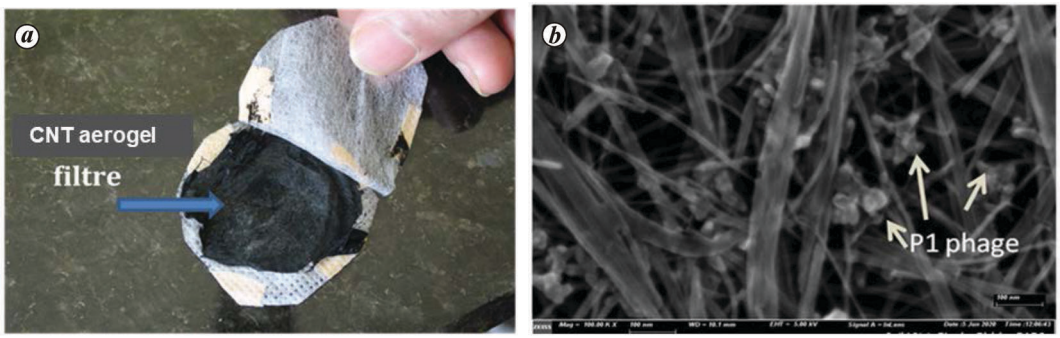

Figure 25. ***a***, Filter made from CNT aerogel. ***b***, SEM image showing P1 phage trapped in the filter.

electrical properties, therefore providing ultra-high sensitivity and specificity toward biomolecules (Figure 26 *a*–*e*).

Using this device, the target DNA hybridization was detected by a quantifiable change in the electrochemical impedance, with a distinct response to the single-stranded probe alone or double-stranded target–probe complex. The target DNA was specifically detected with a limit of detection of 1 pM with a turnaround time of less than 20 min. Moreover, this system is able to differentiate between the closely related target sequences by the distinct impedance response, rendering it highly specific. The detection mechanism of the CNT aerogel electrode works on the principle of π–π interactions between negatively charged single-stranded DNA and CNT.

From the above discussions and illustrations, it is obvious that carbon-based materials can be used for a gamut of applications as their structures and properties can be tailored depending on the requirements. There are challenges in developing the technologies, and BARC has been successful in overcoming these challenges and in the large-scale deployment of a few of the technologies.

Summary and future roadmap

The programme of indigenous materials development at BARC started with the aim of becoming self-reliant in nuclear materials. The expertise developed by the Materials Group, BARC, in the fields of hydrometallurgical, electrometallurgical and pyrometallurgical processing of materials was a key to meet the demands of materials for India's nuclear power programme. This extensive expertise in metallurgy and materials engineering at the Materials Group, BARC, also led to the development of spin-off technologies for non-nuclear applications. Starting from refractory materials to rare earths to recycling of e-waste to recover rare earths, hazardous and valuable materials,

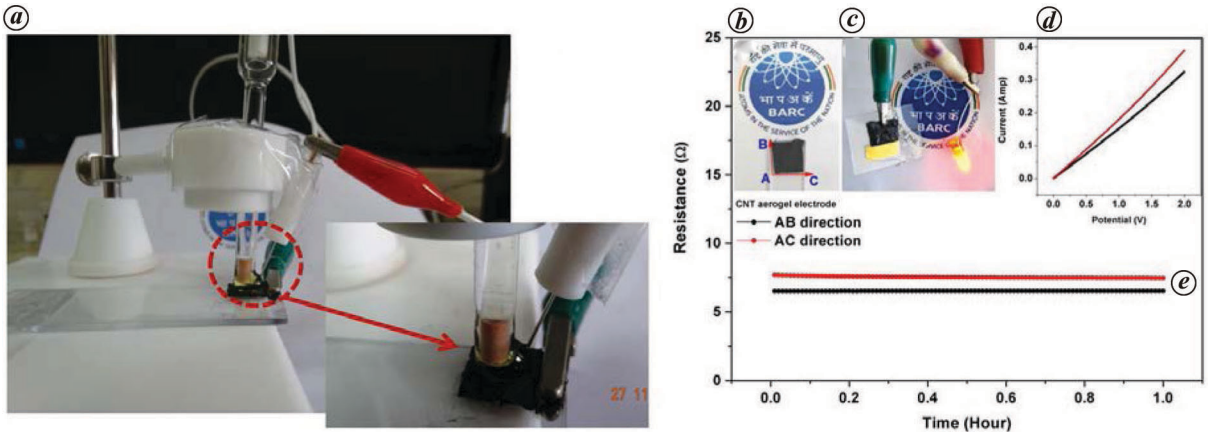

Figure 26. ***a***, Electrochemical impedance system for biosensing. ***b***, CNT aerogel electrode. ***c***, Conductivity test. ***d***, IV curve. ***e***, Chronoamperometry test of CNT aerogel electrode (reproduced from ref. 21).

the Materials Group at BARC has developed technologies for a wide range of the elements in the periodic table. Among these technologies, two examples have been elaborated. The technology of Ni–Ti-based SMA has been utilized in the LCA Tejas, whereas carbon nanomaterials-based technology has been utilized in the light-weight ballistic resistant jacket Bhabha Kavach. The success is based on the detailed understanding of the structure–property correlation in these complex systems at the atomic/molecular level, and further generation of engineering database for the scale-up of these technologies. Such an approach ensures many more developments of technologies in the future – to meet the requirements of India's nuclear power programme as well as spin-off technologies.

1. Krishnan, M. The self accommodating martensitic microstructure of Ni–Ti shape memory alloys. *Acta Mater.*, 1997, **46**, 1439–1457.
2. Krishnan, M. and Singh, J. B., A novel B19′ martensite in nickel titanium shape memory alloys. *Acta Mater.*, 2000, **48**, 1325–1344.
3. Krishnan, M., Maji, B. C. and Banerjee, S., The application of Ni–Ti shape memory alloys as fasteners. *Miner. Process. Extract. Metall. Rev.*, 2001, **22**, 341–367.
4. Krishnan, M., Shape memory alloys. *BARC Newsl.*, 2009, **309**, 19–24.
5. Nightingale, R. E. (ed.), Graphite in nuclear industry. In *Nuclear Graphite*, Academic Press, New York, USA, 1962, pp. 1–20.
6. Dulera, I. V., Sinha, R. K., Rama Rao, A. and Patel, R. J., High temperature reactor technology development in India. *Prog. Nucl. Energy*, 2017, **101**, 82–99.
7. Dasgupta, K., Joshi, J. B., Singh, H. and Banerjee, S., Fluidized bed synthesis of carbon nanotubes: reaction mechanism, rate controlling step and overall rate of reaction. *AIChE J.*, 2014, **60**, 2882–2892.
8. Alexander, R., Ravikanth, K. V., Srivastava, A. P., Krishnan, M. and Dasgupta, K., Synergistic effect of carbon nanotubes on the properties of hot pressed boron carbide. *Mater. Today Commun.*, 2018, **17**, 450–457.
9. Dasgupta, K., Prakash, J., Srivastava, D., Dey, G. K. and Basu, S., A process for fabricating carbon nanotube incorporated ballistic resistant armour panels and products thereof – Indian Patent App No. 201721015925 dated 5 May 2017.
10. Dasgupta, K., Role of carbon nanotubes in the ballistic properties of boron carbide/carbon nanotube/ultrahigh molecular weight polyethylene composite armor. *Ceramic Int.*, 2020, **46**, 4137–4141.
11. Yadav, K. K., Dasgupta, K., Singh, D. K., Anitha, M., Varshney, L. and Singh, H., Solvent impregnated carbon nanotube embedded polymeric composite beads: an environment benign approach to the separation of rare earths. *Sep. Purif. Technol.*, 2015, **143**, 115–124.
12. Yadav, K. K., Dasgupta, K., Singh, D. K., Varshney, L. and Singh, H., Dysprosium sorption by polymeric composite bead: robust parametric optimization using Taguchi method. *J. Chromatogr. A*, 2015, **1384**, 37–43.
13. Singha Deb, A. *et al.*, Carbon nanotubes functionalized with novel functional group amido-amine for sorption of actinides. *J. Hazard. Mater.*, 2018, **345**, 63–75.
14. Sengupta, A., Singha Deb, A. K., Dasgupta, K., Adya, V. C. and Ali, Sk. M., Diglycolamic acid functionalized multiwalled carbon nanotube highly efficient sorbent for f-block elements: experimental and theoretical investigation. *New J. Chem.*, 2017, **41**, 4531–4545.
15. Kumar, P., Sengupta, A., Singha Deb, A., Dasgupta, K. and Ali, Sk. M., Sorption behaviour of Pu^{4+} and PuO_2^{2+} on amido amine functionalized carbon nanotube: experimental and computational study. *RSC Adv.*, 2016, **6**, 107011–107020.
16. Kar, S., Bindal, R. C., Prabhakar, S., Tewari, P. K., Dasgupta, K. and Sathiyamoorthy, D., Potential of carbon nanotubes in water purification: an approach towards the development of an integrated membrane system. *Int. J. Nucl. Desalin.*, 2008, **3**, 143–150.
17. Kar, S., Bindal, R. C. and Tewari, P. K., Carbon nanotube membranes for desalination and water purification: challenges and opportunities. *Nano Today*, 2012, **7**, 385–389.
18. Dasgupta, K. *et al.*, Self-standing geometry of aligned carbon nanotubes with high surface area. *Mater. Lett.*, 2008, **62**, 1989–1992.
19. Yadav, M. D. and Dasgupta, K., Role of sulfur source on the structure of carbon nanotube cotton synthesized by floating catalyst chemical vapour deposition. *Chem. Phys. Lett.*, 2020, **748**, 137391.
20. Alexander, R., Prakash, J., Kaushal, A. and Dasgupta, K., Confocal Raman spectroscopy of carbon nanomaterials. *Phys. News*, 2020, **50**, 28–31.
21. Prakash, J., Dey, A., Uppal, S., Alexander, R., Kaushal, A., Misra, H. S. and Dasgupta, K., Label-free rapid electrochemical detection of DNA hybridization using ultrasensitive standalone CNT aerogel biosensor. *Biosens. Bioelectron.*, 2021, **191**, 113480.

doi: 10.18520/cs/v123/i3/417-428